Australasian Physical & Engineering Sciences in Medicine (2019) 42:511–528
https://doi.org/10.1007/s13246-019-00752-7

SCIENTIFIC PAPER

A comparative study between normal electrocardiogram signal and those of some cardiac arrhythmias based on McSharry mathematical model

Pascalin Tiam Kapen[1,2] · Serge Urbain Kouam Kouam[2] · Ghislain Tchuen[2]

Received: 3 September 2018 / Accepted: 27 March 2019 / Published online: 2 April 2019

Abstract
In this paper, synthetic electrocardiogram signals (SECG) of eight cardiac arrhythmias (sinus bradycardia, junctional bradycardia, tachycardia, flutter, atrial extrasystole, ventricular extrasystole, left branch block and right branch block) are obtained numerically by solving the McSharry mathematical model (2003) based on three coupled ordinary differential equations with the fourth-order Runge–Kutta method. They are compared with normal electrocardiogram signal. Indeed, visual analysis of a section of electrocardiogram (ECG) signals of these arrhythmias was used to suggest suitable values for the parameters in the McSharry mathematical model. Results from numerical simulation showed a good agreement between the simulation results and the real cardiac arrhythmias ECG signals.

Keywords Synthetic electrocardiogram signals · Cardiac arrhythmias · McSharry mathematical model

Introduction

An ECG is a measure of how the electrical activity of the heart changes in the myocardium during each cardiac cycle. It is obtained by recording the potential difference between two electrodes placed on the surface of the skin (the negative electrode placed on the right wrist, and the positive electrode placed on the left ankle for a typical lead II ECG). In response to action potentials moving along the chambers of the heart, the heart contracts during the cardiac cycle. At the same time, one part of the cardiac tissue is depolarized and another part is at rest or polarized. These successive depolarization/repolarization (atrial or ventricular) are generally associated with the peaks and troughs of the ECG waveform namely P, Q, R, S and T.

The main information that provides precisions about the quality of the cardiac signal is contained in the PQRST-complex (Fig. 1). Therefore, several methods have been proposed in the literature to extract this clinical information. Among the most widely used are the Haar wavelets [1, 2], the Mexican hat [3, 4], the Morlet wavelets [5, 6], the quadratic spline wavelets [7] or even their combination [8]. In addition, different algorithms have been developed for the detection of the QRS complex [9–16]. Numerous modeling techniques including different aspects of the heart rhythms by means of different types of mathematical models have also been proposed (Holden and Poole [17], Boyett et al. [18], Holden and Biktashev [19], Poole et al. [20], Gois and Savi [21], Tlili et al. [22], Wu et al. [23]). Recently, a novel method for the detection and classification of life-threatening ventricular arrhythmia episodes has been formulated [24]. Indeed, it decomposes the ECG signal into various oscillatory modes using digital Taylor–Fourier transform (DTFT). Another recent algorithm using the sparse representation technique has been developed. Here, an overcomplete gabor dictionary is used for the decomposition of the ECG signal into elementary waves [25]. In addition, the use of supervised machine learning for the detection in ECG patterns has been widely demonstrated [26, 27]. Moreover, a mathematical model for generating a SECG signal with realistic PQRST morphology and prescribed heart rate dynamics has been constructed [29]. It provides a standard realistic ECG signal with known characteristics, which can be generated with specific statistics such as the mean and standard deviation

✉ Pascalin Tiam Kapen
ptiam@udm.aed-cm.org

[1] Université des Montagnes, ISST, P.O. Box 208, Bangangté, Cameroon

[2] University of Dschang, LISIE/L2MSP, P.O. Box 134, Bandjoun, Cameroon

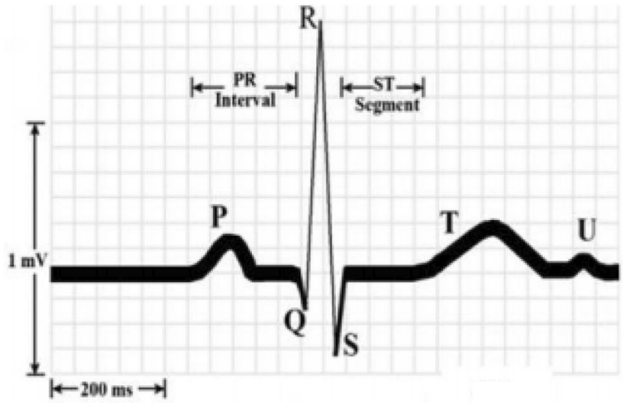

Fig. 1 Normal ECG showing PQRST-complex

of the heart rate and frequency-domain characteristics of the heart rate variability, for instance, low-frequency/high frequency ratio. This paper extends this mathematical model for the generation of SECG of eight cardiac arrhythmias (sinus bradycardia, junctional bradycardia, tachycardia, flutter, atrial extrasystole, ventricular extrasystole, left branch block and right branch block) by finding specific parameter values of the model.

This paper is structured as follows. "Cardiac conduction system" section gives some fundamentals about the cardiac conduction system and some cardiac arrhythmias. "Mathematical modeling" section presents the mathematical background. In "Numerical results" section, the numerical results are shown and "Conclusion" section concludes and gives some perspectives.

Cardiac conduction system

Strands and clumps of specialized cardiac muscle contain only a few myofibrils and are located throughout the heart. They initiate and distribute impulses through the myocardium, comprising the cardiac conduction system that coordinates the cardiac cycle (Fig. 2). The sinoatrial node (SA node) is a small mass of specialized tissue just beneath the epicardium, in the right atrium. The SA node's cells can reach threshold on their own, initiating impulses through the myocardium, stimulating contraction of cardiac muscle fibers. Since it generates the heart's rhythmic contractions, it is often referred to as the pacemaker. The path of a cardiac impulse travels from the SA node into the atrial syncytium, and atria begin to contract almost simultaneously. The impulse passes along junctional fibers of the conduction system to a mass of specialized tissue called the atrioventricular node (AV node), located in the inferior interatrial septum, beneath the endocardium. The AV node provides the only normal conduction pathway between the atrial and ventricular syncytia. When the cardiac impulse reaches the distal AV node, it passes into a large AV bundle, entering the upper part of the interventricular septum. Nearly halfway down

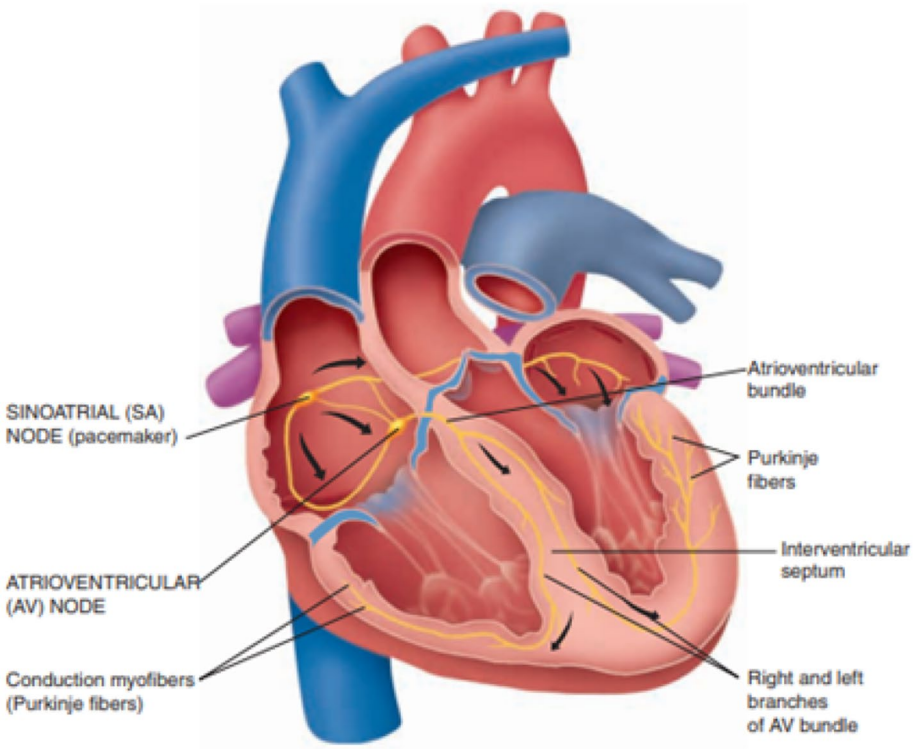

Fig. 2 The cardiac conduction system [28]

the septum, these branches spread into enlarged Purkinje fibers (Fig. 2) [28].

The ECG signal is therefore generated and contains the following waves:

- P wave which represents the atrial depolarization. It generally lasts between 60 and 90 ms for normal adults and has a maximum amplitude between 0.25 and 0.30 mV.
- QRS-complex which corresponds to ventricular depolarization. It lasts about 80 ms.
- T wave which represents the ventricular repolarization. It has an amplitude about 0.60 mV.

Cardiac arrhythmias

Sinus bradycardia

Bradycardia is a pathology caused by an abnormal heart frequency (less than 60 Bpm). It arises when the site of initiation of the electrical impulse at the origin of the beats is in the atria. Figure 3 shows a real sinus bradycardia ECG signal.

Junctional bradycardia

In case of sinus dysfunction with or without atrial depolarization, the AV node can act as a backup pacemaker at a frequency in the range of 30 to 60 Bpm. The electrical impulse then originates in the atrioventricular (AV) node and follows the usual conduction path. The morphology of QRS waves is different from that of normal beat, and, the P wave may be absent or, if present, it may be out of sync with ventricular systole. Figure 4 presents a junctional bradycardia ECG signal.

Tachycardia

In contrast to bradycardia, tachycardia is characterized by a high heart frequency (greater than 100 Bpm). It can be of sinus, atrial or ventricular origin. However, any irregularity here is not pathological because in situations of stress or physical effort, the autonomic nervous system exercising permanent control, can greatly accelerate the pace in response to a particular context. It is therefore important to consider the patient's activity before making a diagnosis. Figure 5 presents a tachycardia ECG signal.

Flutter

Flutter is a pathology caused by the disorder of the heart rhythm. It can be of atrial (atrial flutter) or ventricular (ventricular flutter) origin. It is due to the lack of synchronization between the SA node and the AV node and characterized by a very high frequency. The most frequently flutter encountered (90% of cases) is the atrial flutter. The frequency being so high (300 Bpm in the case of atrial flutter), the cardiac system is not in the possibility to drive all the electrical pulses generated. The flutter ECG signal is presented in Fig. 6.

Atrial extrasystole

Extrasystole or prematurity is a cardiac rhythm disorder corresponding to a premature contraction of one of the cavities of the heart. It occurs when the membrane depolarization comes from a place other than sinus node. Depending on the cardiac cavity where the premature contraction of the muscular fibers occurs, atrial extrasystoles (ESAs), ventricular extrasystoles (VES) or junctional

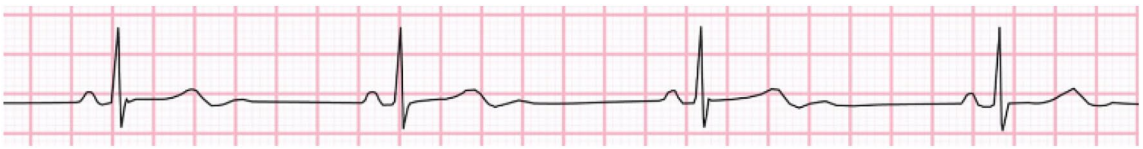

Fig. 3 Sinus bradycardia ECG signal

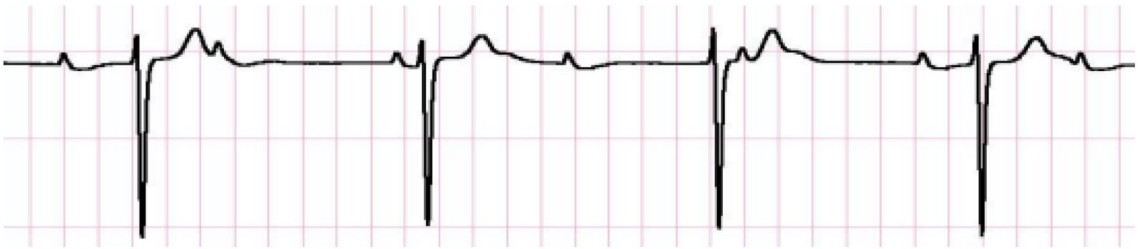

Fig. 4 Junctional bradycardia ECG signal

extrasystoles are referred to respectively. It is normal to have some extrasystoles a day. Their number increases with age, and it is usual to count, for example, nearly 1000 atrial extrasystoles per 24 h in an octogenarian without this having any significance. They become worrying and can lead to fibrillation or tachycardia if they appear more than six times per minute (360 per hour) or incurred if there are more than 200 polymorphous extrasystoles per hour. Extrasystoles can be caused by stress, excitants, cardiopathy: myocardial ischemia, myocarditis, dilated or hypertrophic cardiomyopathy, hiatal hernia and significant physical exertion. The ECG of the atrial extrasystole is characterized by a premature P wave with variable morphology depending on the starting point in the atria. Depending on the time of prematurity, the impulse generated can be blocked either in the AV node or in one of the branches of the His bundle. Figure 7 shows the atrial extrasystole ECG signal.

Ventricular extrasystole

In this case, the electrical signal propagates out of the physiologic conduction pathways through myocardial tissue. Generally, the P wave is absent and the morphology of the QRS complex depends on the location of the ectopic focus that can be anywhere in the ventricles. The QRS complex is deformed compared to the normal one (Fig. 8).

Left branch block

The electrical signal leaving the AV node propagates simultaneously in the two branches of the His bundle (left branch

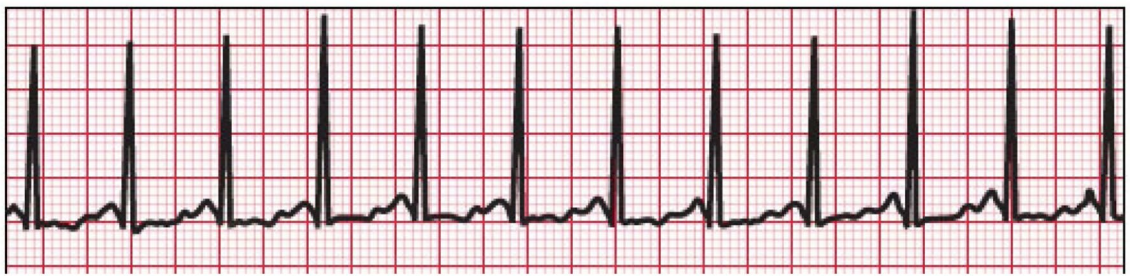

Fig. 5 Tachycardia ECG signal

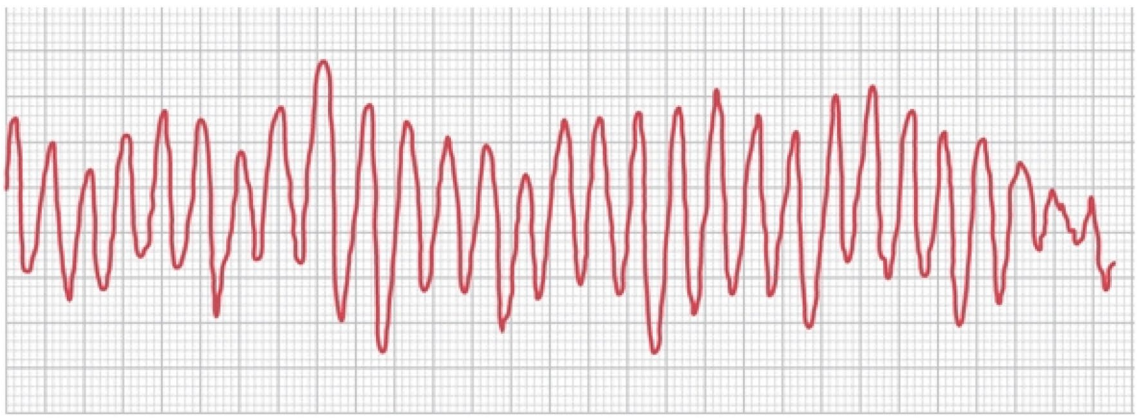

Fig. 6 Flutter ECG signal

Fig. 7 Atrial extrasystole ECG signal

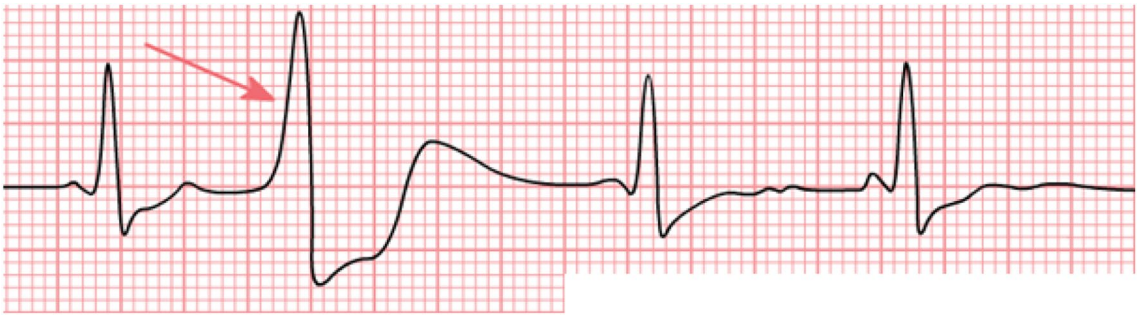

Fig. 8 Ventricular extrasystole ECG signal

and right branch) and then in the branches of the Purkinje networks. Depending on the side of the branch where the interruption of signal conduction occurs, the left branch block (BBD) and the right branch block (BBG) will be distinguished. The left branch block occurs when there is conduction defect on the left branch of the His bundle (Fig. 9).

Right branch block

In contrast to the left branch block, the right branch block occurs when the conduction on the right branch of the His bundle is interrupted. The influx passes through the left branch, and then the transmission continues through the Purkinje fibers to the right ventricle (Fig. 10).

Mathematical modeling

The dynamical model used in this work is the one proposed by McSharry [29]. It generates a trajectory in a three-dimensional state-space with coordinates (x, y, z) (Fig. 11). The different points on the ECG signal (P, Q, R, S and T) are described by events which are placed at fixed angles along the unit circle given by $\theta_P, \theta_Q, \theta_R, \theta_S$ and θ_T.

Its mathematical formulation reads

$$\begin{cases} \dot{x} = \alpha x - \omega y \\ \dot{y} = \alpha y + \omega x \\ \dot{z} = -\sum\limits_{i\in\{P,Q,R,S,T\}} a_i \Delta\theta_i exp\left(-\frac{\Delta\theta_i^2}{2b_i^2}\right) - \left(z - z_0\right) \end{cases} \tag{1}$$

with $\alpha = 1 - \sqrt{x^2 + y^2}$, $\Delta\theta_i = \left(\theta - \theta_i\right) \bmod 2\pi$, $\theta = atan2(y, x)$.

ω is the angular velocity of the trajectory as it moves around the cycle limit. The baseline value $z_0(t)$ is defined by

$$z_0(t) = Z_m \sin\left(2\pi f_0 t\right) \tag{2}$$

where f_0 is the respiratory frequency and $Z_m = 0.15\,\text{mV}$.

The parameters used in [29] for normal ECG signal are given in Table 1.

The Runge–Kutta numerical method was used to solve Eq. (1). Indeed, system (1) can be rewritten as:

$$\frac{d\vec{U}}{dt} = \vec{f}(t, x, y) \tag{3}$$

where $\vec{U}\begin{pmatrix} x \\ y \\ z \end{pmatrix}$ and $\vec{f}_{(t,x,y)} = \begin{pmatrix} \alpha x - \omega y \\ \alpha y + \omega x \\ -\sum\limits_{i\in\{P,Q,R,S,T\}} a_i \Delta\theta_i exp\left(-\frac{\Delta\theta_i^2}{2b_i^2}\right) - \left(z - z_0\right) \end{pmatrix}$

Then, the Runge–Kutta method for this system is given by the following equations:

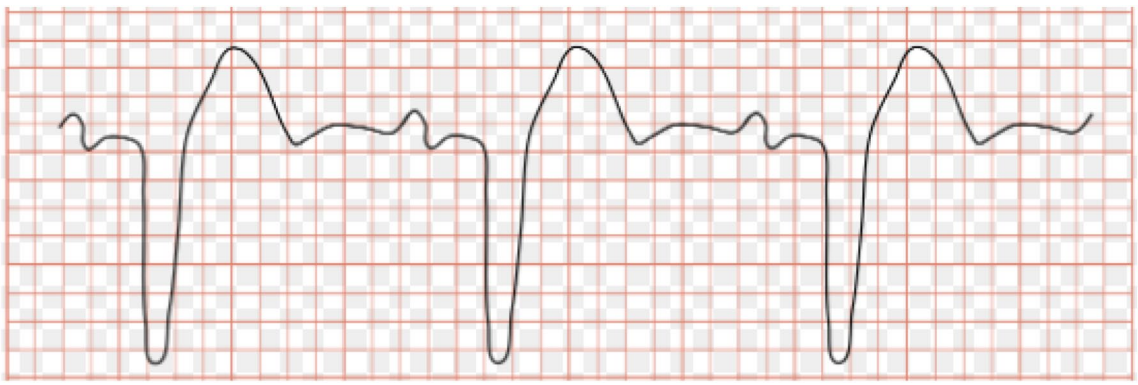

Fig. 9 Left branch block ECG signal

Fig. 10 Right branch block ECG signal

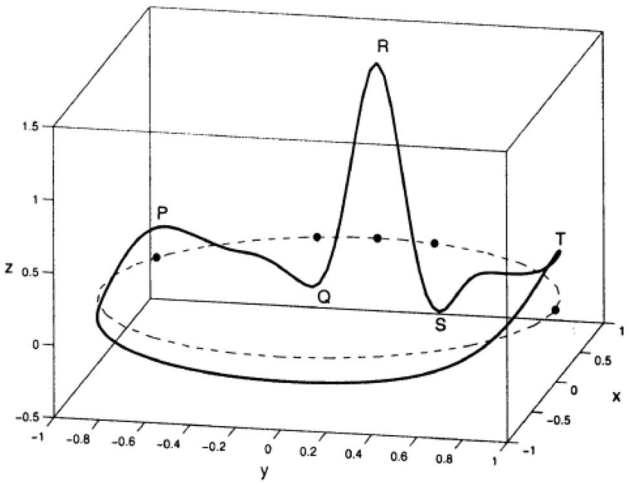

Fig. 11 The trajectory in a 3D state-space

Table 1 Parameter values of the normal ECG signal used in [29]

Index (i)	P	Q	R	S	T
Time (s)	−0.2	−0.05	0	0.05	0.3
θ_i (radians)	$-\frac{\pi}{3}$	$-\frac{\pi}{12}$	0	$\frac{\pi}{12}$	$\frac{\pi}{2}$
a_i	1.2	−5.0	30.0	−7.5	0.75
b_i	0.25	0.1	0.1	0.1	0.4
ω	2π				

$$\vec{U}_{n+1} = \vec{U}_n + \frac{h}{6}\left(\vec{k}_1 + 2\vec{k}_2 + 2\vec{k}_3 + \vec{k}_4\right) \tag{4}$$

$$t_{n+1} = t_n + h \tag{5}$$

with h the time step. Concerning the quantities $\vec{k}_1, \vec{k}_2, \vec{k}_3$, and $\vec{k}_4$, they read:

$$\vec{k}_1 = \vec{f}\left(t_n, \vec{U}_n\right) \tag{6}$$

$$\vec{k}_2 = \vec{f}\left(t_n + \frac{h}{2}, \vec{U}_n + \frac{h\vec{k}_1}{2}\right) \tag{7}$$

$$\vec{k}_3 = \vec{f}\left(t_n + \frac{h}{2}, \vec{U}_n + \frac{h\vec{k}_2}{2}\right) \tag{8}$$

$$\vec{k}_4 = \vec{f}\left(t_n + h, \vec{U}_n + h\vec{k}_3\right) \tag{9}$$

Therefore, parameters values are now deduced considering the physical meaning of each signal. Indeed, they are found by varying key parameters in the interval characterizing each pathology. The flowchart of the Runge–Kutta method of order 4 is as follows (Fig. 12).

Numerical results

Visual analysis of a section of electrocardiogram (ECG) signals of the presented arrhythmias was used to suggest suitable values for the parameters in the McSharry mathematical model. Figure 13a shows the normal ECG signal generated with the values of Table 1. Figure 13b shows the normal ECG signal of the MIT database [30].

Tables 2, 3, 4, 5, 6, 7, 8 and 9 summarize the parameters values used to generate the ECG for cardiac arrhythmias. The modified values are in bold.

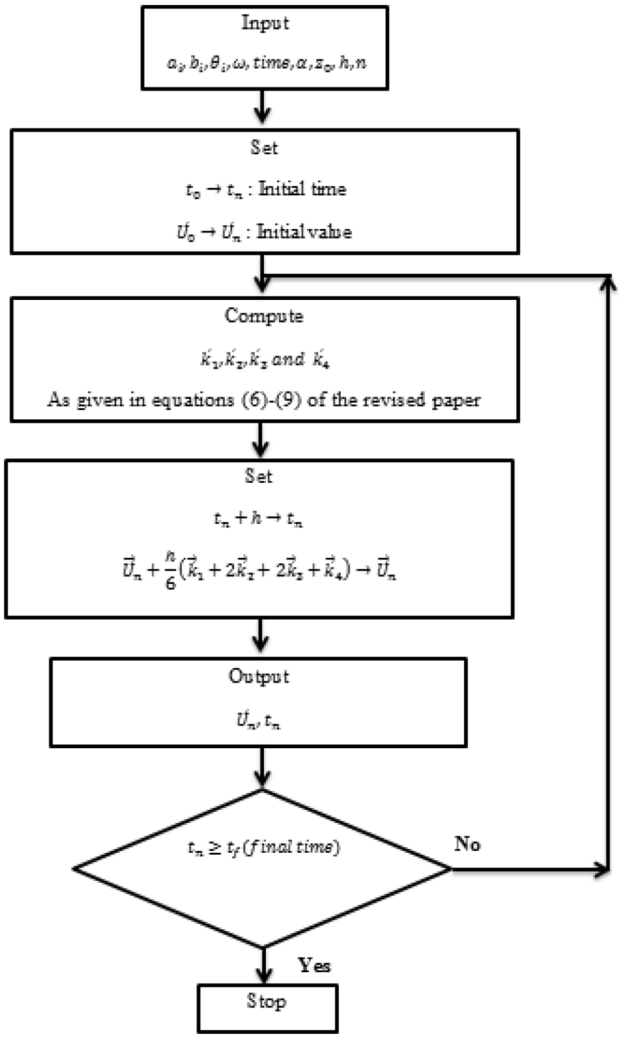

Fig. 12 Flowchart of the Runge–Kutta method of order 4

Discussion

Figure 14a, b present the generated ECG signal for sinus bradycardia and from MIT database respectively. It can be noticed the presence of waves P, Q, R, S and T. These waves have the same morphology as those of the normal ECG which is justified by the fact that for this pathology, the electrical signal follows the same path during a normal beat. It is noted that the period of the pathological signal is lower than that of the normal signal. In our case, the heart frequency is 40 Bpm. The two signals presented in Fig. 14 are in good agreement.

In Fig. 15a, b, we observe on the pathological ECG, the presence of the P wave which is desynchronized because it is the AV node that provides the pacemaker function. Therefore, the electrical activity of the atria and those of the ventricles are not synchronized. The frequency of the pathological signal is lower than the normal frequency because the new pacemaker (the AV node) can only generate a heart frequency in the range of 30 to 60 Bpm. In this case, the frequency is 30 Bpm.

Figure 16a, b show the ECG signal for tachycardia where it can be observed a higher frequency compared to that of the normal signal. In this case, the frequency is 150 Bpm $\left(\frac{10\pi}{3} \leq \omega < 10\pi\right)$. It can be also concluded that the waves have the same morphology as those of the normal ECG signal.

At a frequency greater than or equal to 300 Bpm, the AV node cannot transmit all the signals received. Therefore, it is a lack of synchronization between atria and ventricles because in most cases, less than a third of the signals generated passes through the AV node. Figure 17a, b illustrate a flutter with a frequency of 300 Bpm.

In Fig. 18a, b, the electrical signal has been generated near the AV node causing depolarization of the atria in the reverse direction, generating a negative P-wave. There is also a decrease in heart frequency because the time taken by the signal to reach the AV node is reduced. The shape of the QRS and T waves is unchanged because, having arrived at the AV node, the signal follows its normal path.

In Fig. 19a, b, the created electrical impulse does not follow the normal conduction path (His bundle), and therefore spreads more slowly in the ventricles. The ventricular contraction thus spreads over time loses its effectiveness, hence the presence of a large QRS complex. The absence of the propagation of the electrical signal in the atria is noted because the signal is generated in one of the halves of the ventricle, hence the absence of the P wave on the pathological synthetic signal. In addition, the ectopic focus is in the right ventricle. The electrical signal then propagates from the right atrium to the left atrium in the opposite direction.

In Fig. 20a, b, the presence of a negative QRS complex is justified by the fact that the signal must leave from the right ventricle to the left ventricle in a reverse direction of normal propagation. Propagation of the electrical signal from the right ventricle to the left ventricle results in a large QRS complex.

In Fig. 21a, b, the repolarization of the ventricle is in the opposite direction. This is observed on the ECG signal by a negative T wave. Moreover, the wave S is not observable on the graph. The initial part of the ECG, namely the P, Q, R and S waves, is not modified.

Conclusion

Synthetic electrocardiogram signals (SECG) of eight cardiac arrhythmias (sinus bradycardia, junctional bradycardia, tachycardia, flutter, atrial extrasystole, ventricular extrasystole, left branch block and right branch block) have been

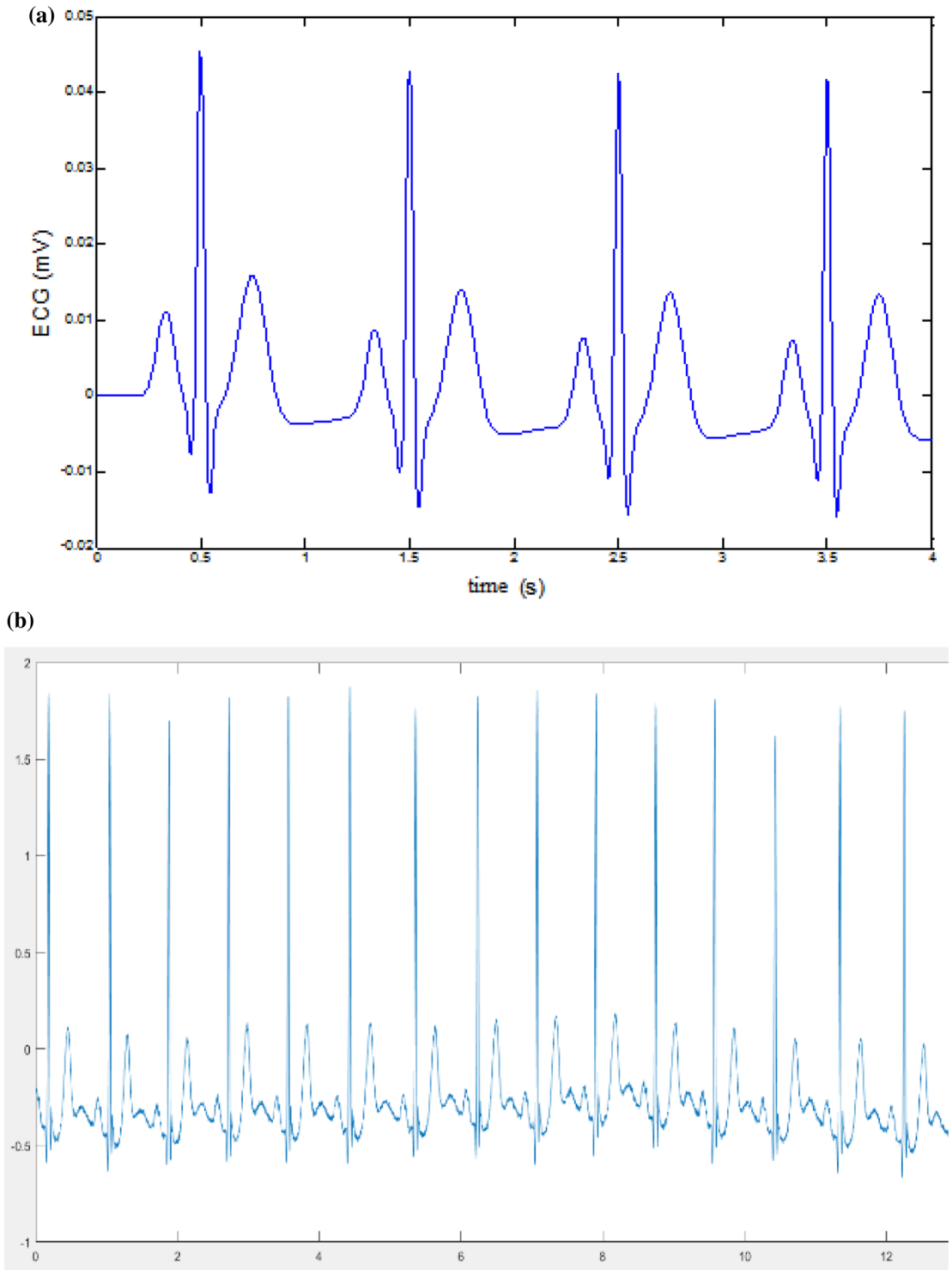

Fig. 13 Normal ECG signal generated from McSharry model (**a**) and from MIT database (**b**)

generated by suggesting suitable values for the parameters in the McSharry mathematical model. They have been compared with those obtained from MIT database. The results show a good agreement. They can be used as a synthetic signals database for educational purposes.

It would be interesting to generate the synthetic ECG signals of more cardiac pathologies to enrich the database. It would be also useful to enrich the work with the quantitative analysis in the future investigation.

Table 2 Parameter values of the sinus bradycardia ECG signal

Index (i)	P	Q	R	S	T
Time (s)	−0.2	−0.05	0	0.05	0.3
θ_i (radians)	$-\frac{\pi}{3}$	$-\frac{\pi}{12}$	0	$\frac{\pi}{12}$	$\frac{\pi}{2}$
a_i	1.2	−5.0	30.0	−7.5	0.75
b_i	0.25	0.1	0.1	0.1	0.4
ω	$\frac{13\pi}{10}$				

Table 3 Parameter values of the junctional bradycardia ECG signal

Index (i)	P	Q	R	S	T
Time (s)	−0.2	−0.05	0	0.05	0.3
θ_i (radians)	$-\frac{2\pi}{3}$	$-\frac{\pi}{12}$	0	$\frac{\pi}{12}$	$-\frac{8\pi}{10}$
a_i	**1.0**	**3.0**	30.0	−7.5	**1.0**
b_i	0.25	0.1	0.1	0.1	0.4
ω	$\frac{3\pi}{2}$				

Table 4 Parameter values of the tachycardia ECG signal

Index (i)	P	Q	R	S	T
Time (s)	−0.2	−0.05	0	0.05	0.3
θ_i (radians)	$-\frac{\pi}{3}$	$-\frac{\pi}{12}$	0	$\frac{\pi}{12}$	$\frac{\pi}{2}$
a_i	1.2	−5.0	30.0	−7.5	0.75
b_i	0.25	0.1	0.1	0.1	0.4
ω	**5π**				

Table 5 Parameter values of the flutter ECG signal

Index (i)	P	Q	R	S	T
Time (s)	−0.2	−0.05	0	0.05	0.3
θ_i (radians)	$-\frac{\pi}{3}$	$-\frac{\pi}{12}$	0	$\frac{\pi}{12}$	0.8
a_i	**10.0**	**20.0**	**25.0**	**19.5**	**10.0**
b_i	0.25	0.1	0.1	**0.17**	**0.25**
ω	**10π**				

Table 6 Parameter values of the atrial extrasystole ECG signal

Index (i)	P	Q	R	S	T
Time (s)	−0.2	−0.05	0	0.05	0.3
θ_i (radians)	$-\frac{3\pi}{4}$	$-\frac{\pi}{12}$	0	$\frac{\pi}{12}$	$\frac{\pi}{2}$
a_i	**−1.2**	−5.0	30.0	−7.5	0.75
b_i	0.25	0.1	0.1	0.1	0.4
ω	**3π**				

Table 7 Parameter values of the ventricular extrasystole ECG signal

Index (i)	P	Q	R	S	T
Time (s)	−0.2	−0.05	0	0.05	0.3
θ_i (radians)	**−0.5π**	$-\frac{\pi}{12}$	0	$\frac{\pi}{12}$	**0.2π**
a_i	**0.2**	−5.0	**−20.0**	**0.2**	**0.31π**
b_i	0.25	0.1	0.1	0.1	0.4
ω	$\frac{7\pi}{2}$				

Table 8 Parameter values of the left branch block ECG signal

Index (i)	P	Q	R	S	T
Time (s)	−0.2	−0.05	0	0.05	0.3
θ_i (radians)	$-\frac{\pi}{3}$	$-\frac{\pi}{12}$	0	$\frac{-3\pi}{15}$	$\frac{\pi}{2}$
a_i	**−0.82**	−5.0	**−30.0**	−7.5	0.75
b_i	0.25	0.1	0.1	0.1	0.4
ω	2π				

Table 9 Parameter values of the right branch block ECG signal

Index (i)	P	Q	R	S	T
Time (s)	−0.2	−0.05	0	0.05	0.3
θ_i (radians)	$-\frac{\pi}{3}$	$-\frac{\pi}{12}$	0	**−0.4π**	**−0.6π**
a_i	1.2	−5.0	30.0	**−0.6**	**−0.3**
b_i	0.25	0.1	0.1	0.1	0.4
ω	2π				

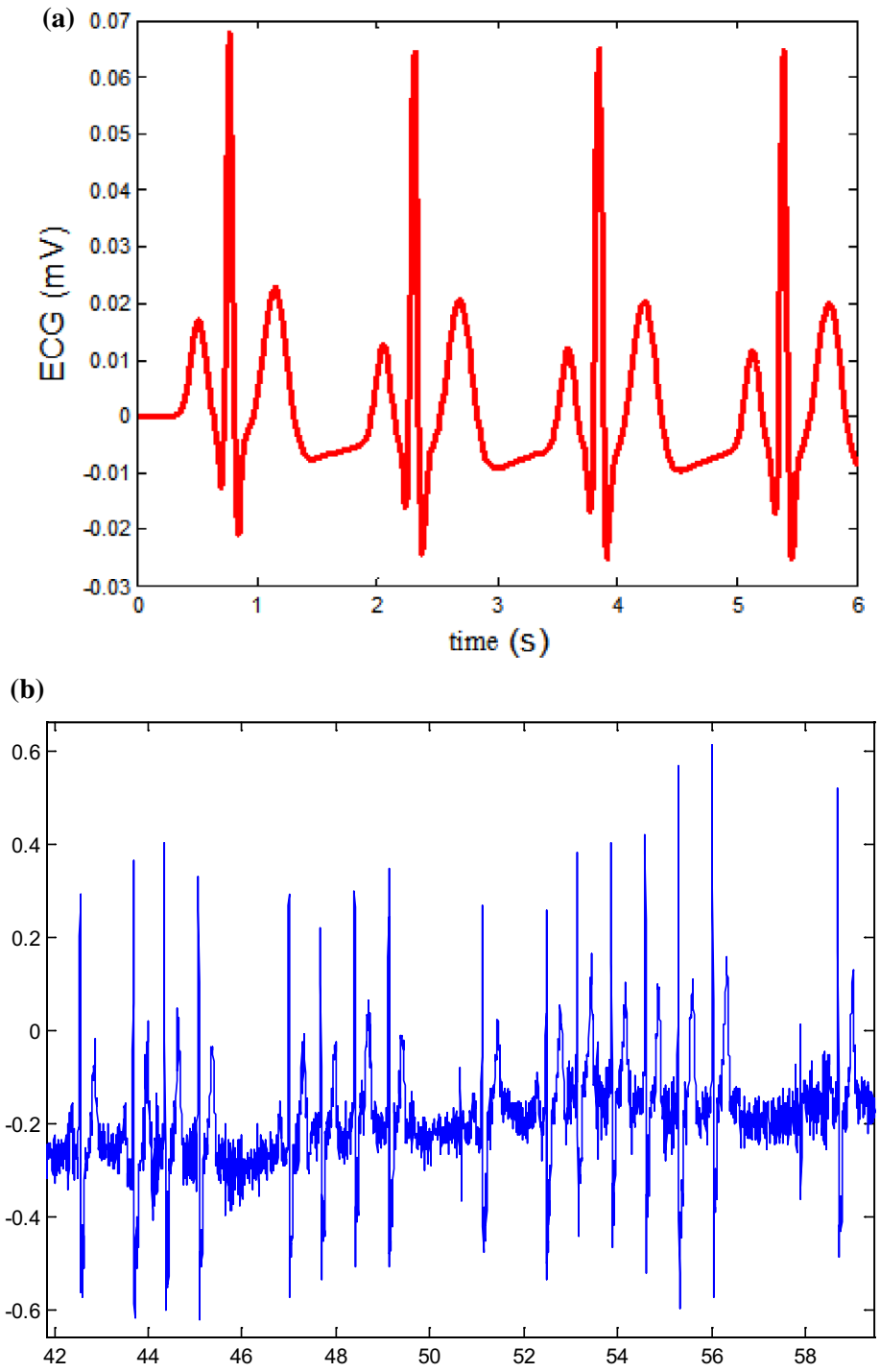

Fig. 14 Simulated sinus bradycardia ECG signal (**a**) and from MIT database (**b**)

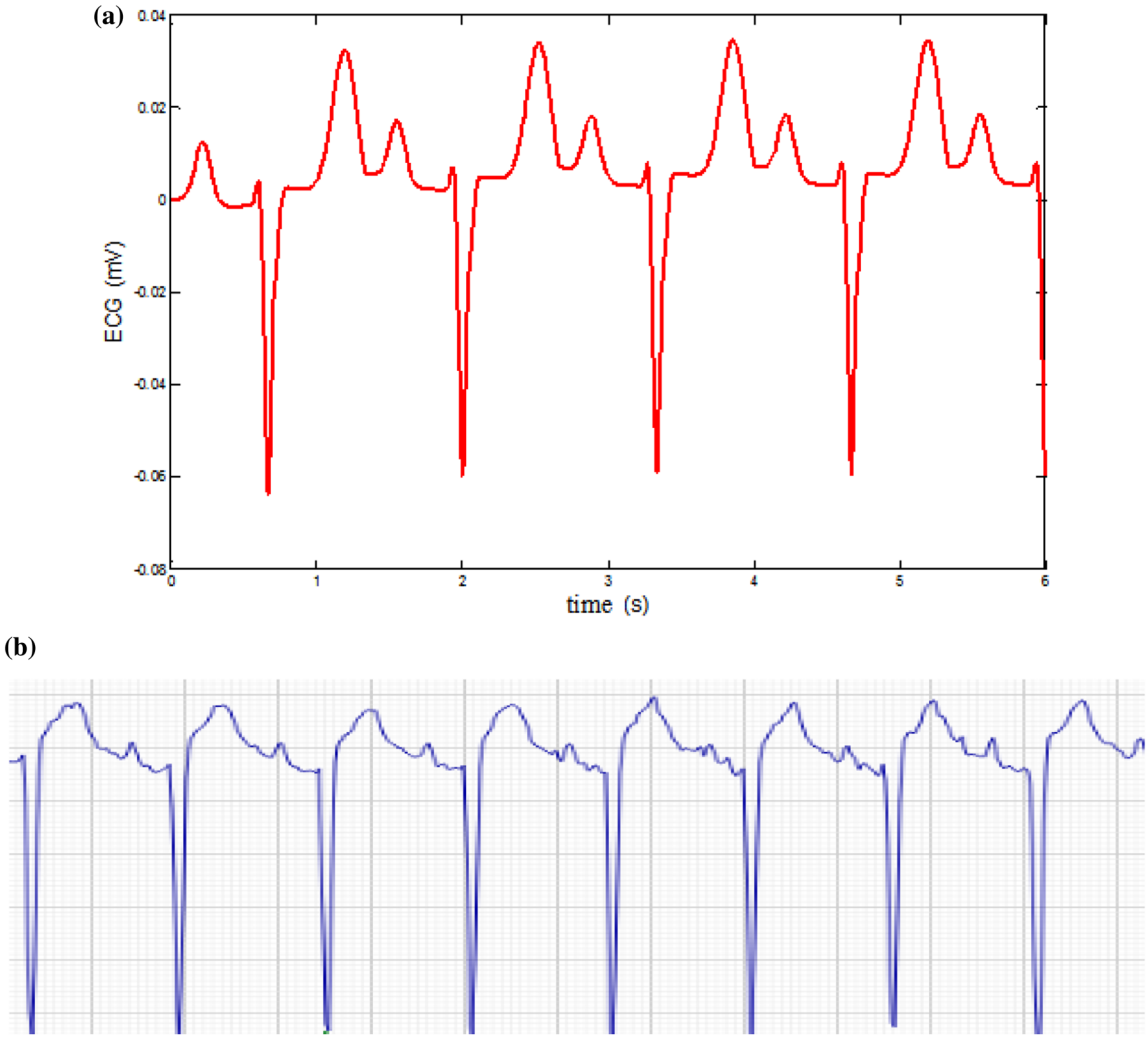

Fig. 15 Simulated junctional bradycardia ECG signal (**a**) and from MIT database (**b**)

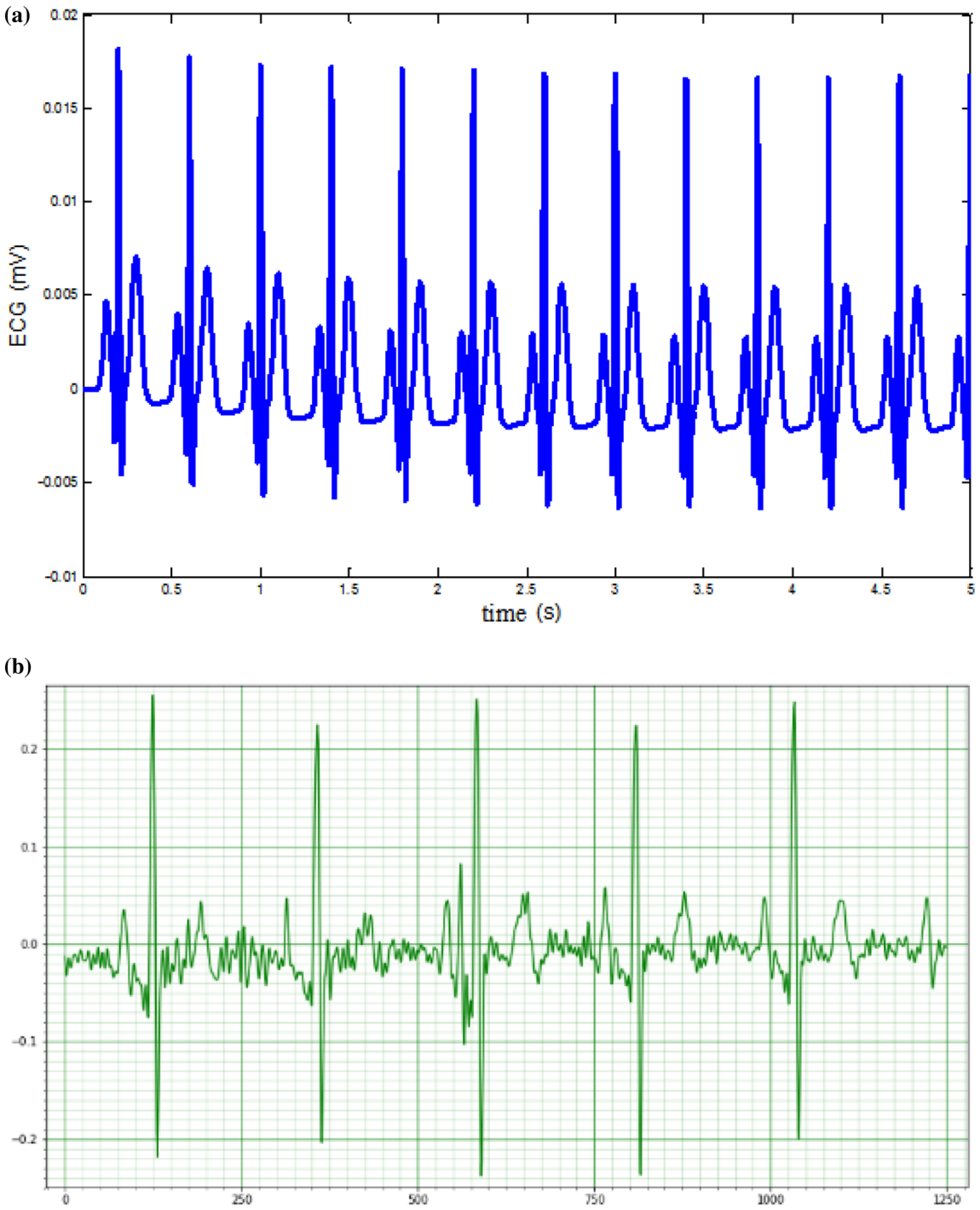

Fig. 16 Simulated tachycardia ECG signal (**a**) and from MIT database (**b**)

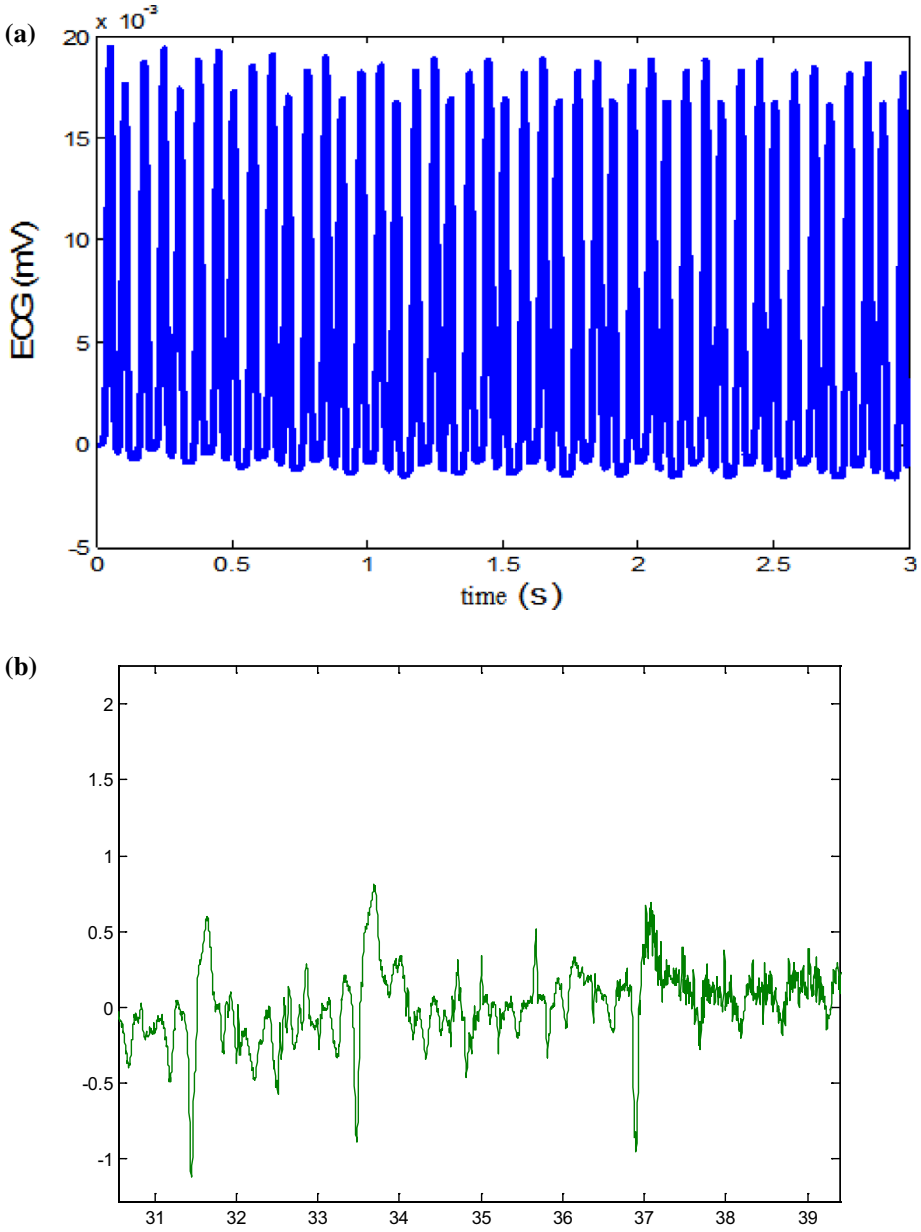

Fig. 17 Simulated flutter ECG signal (**a**) and MIT database signal (**b**)

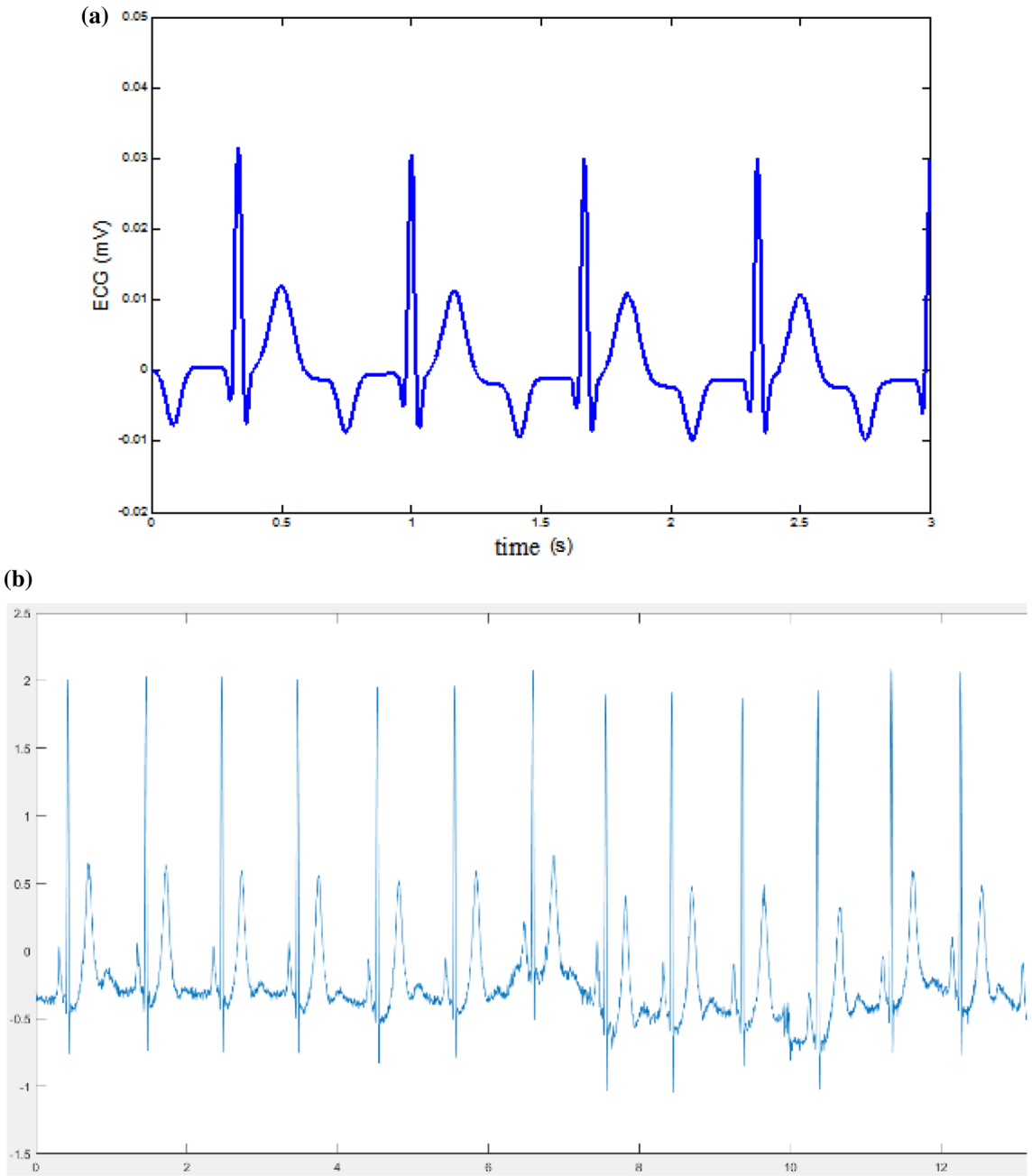

Fig. 18 Simulated atrial extrasystole ECG signal (**a**) and MIT database signal (**b**)

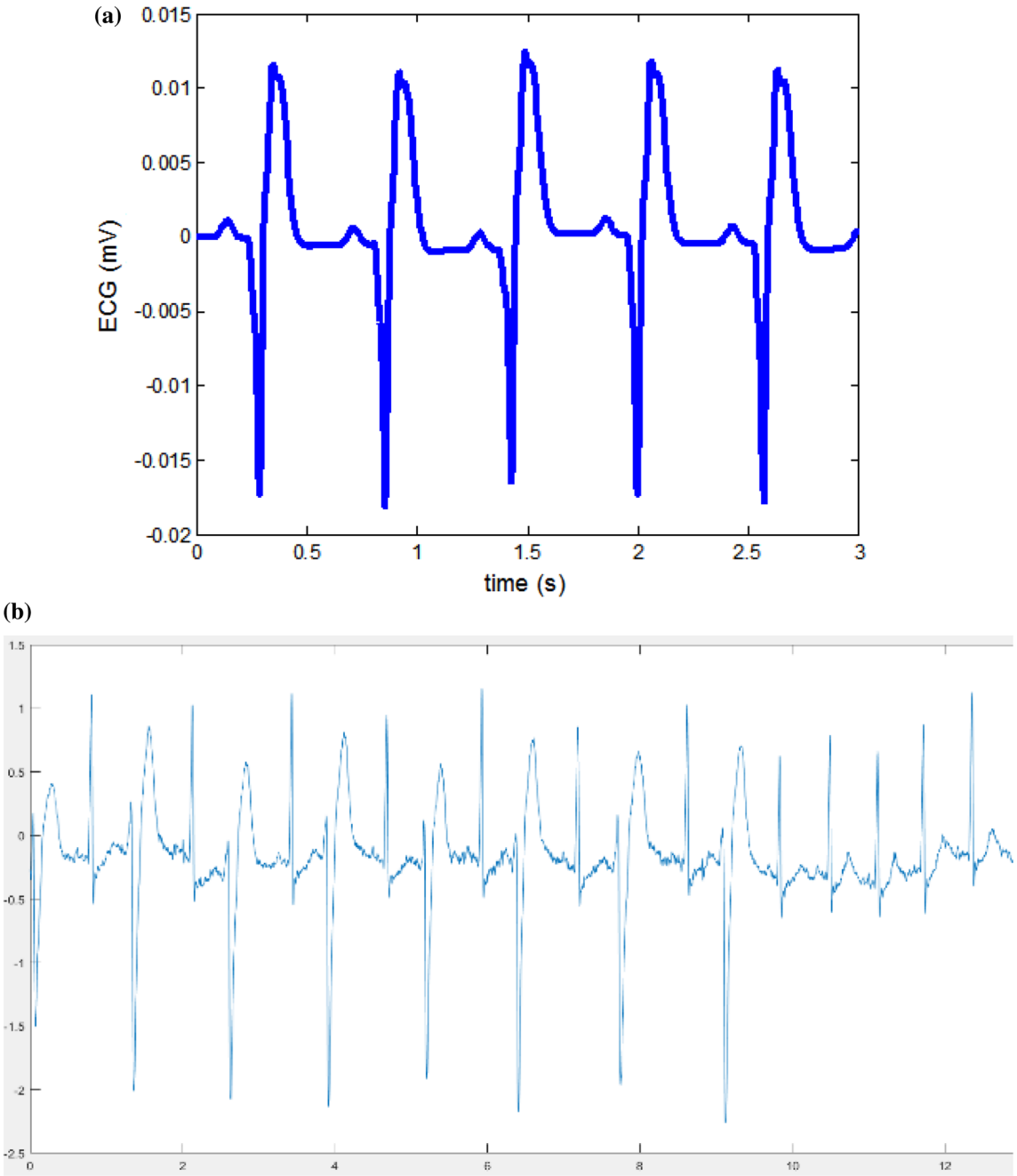

Fig. 19 Simulated ventricular extrasystole ECG signal (**a**) and MIT database signal (**b**)

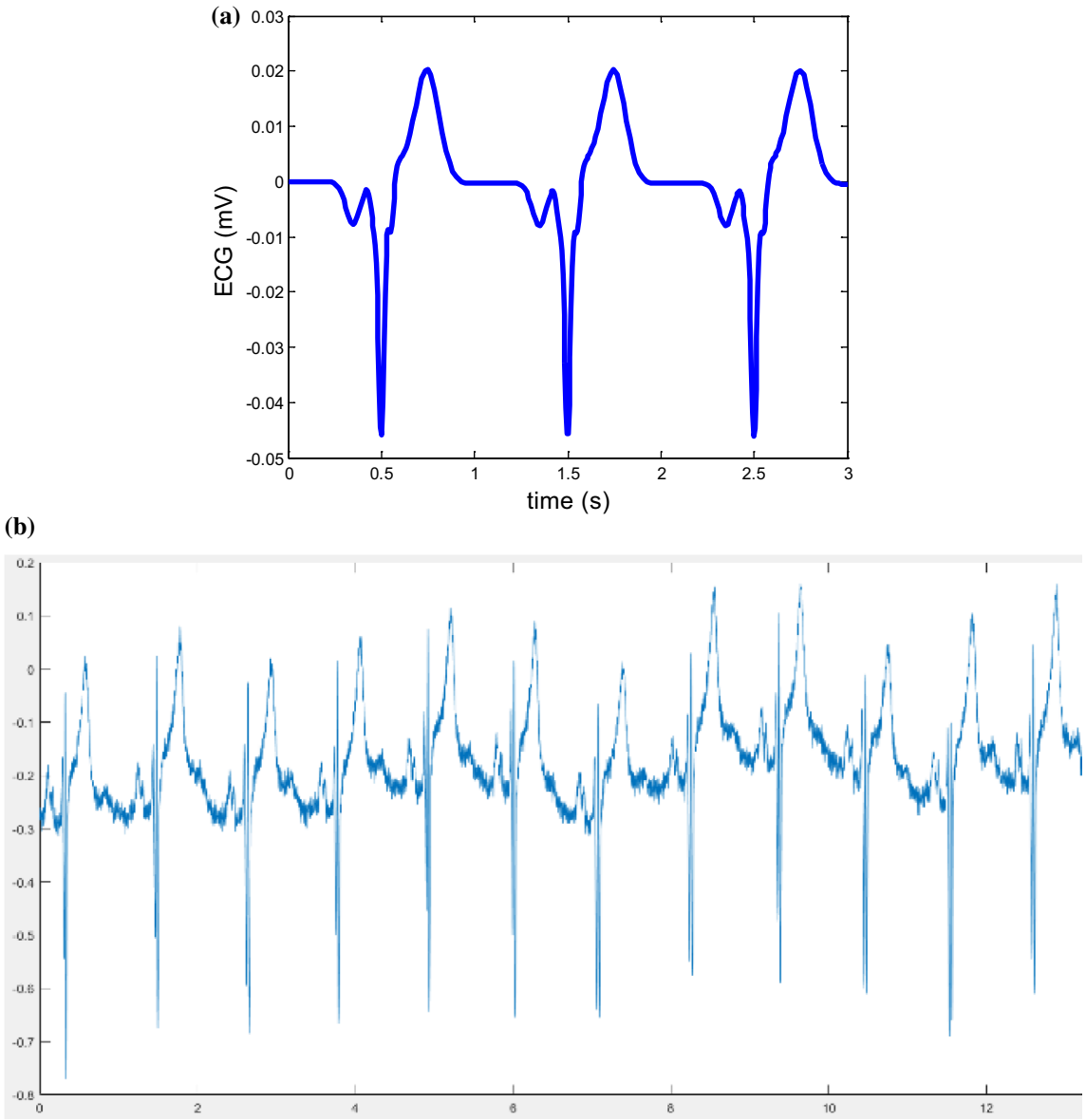

Fig. 20 Simulated left branch block ECG signal (**a**) and MIT database signal (**b**)

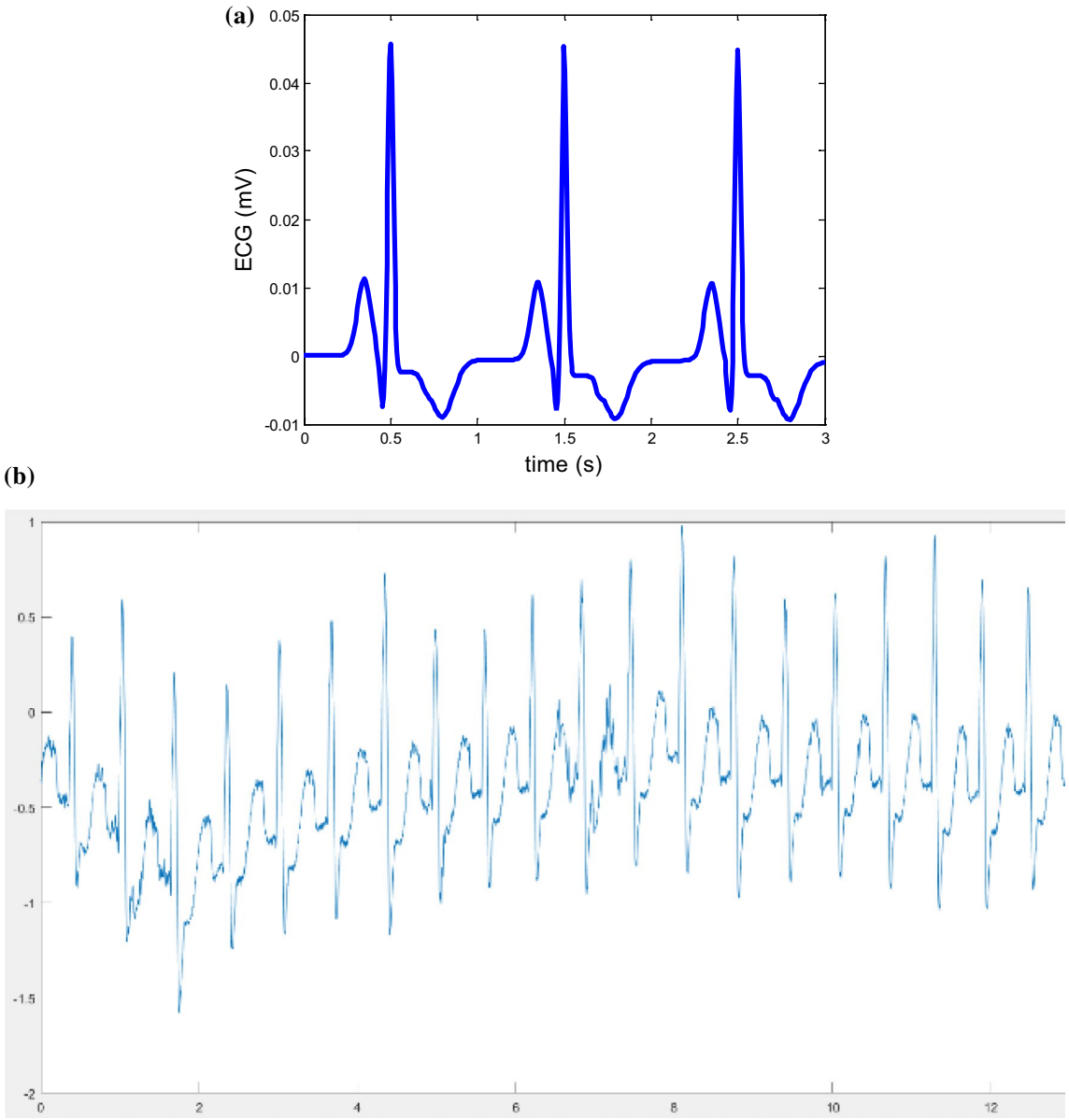

Fig. 21 Simulated right branch block ECG signal (**a**) and MIT database signal (**b**)

Acknowledgements The authors are grateful to Dr. YIAGNIGNI Euloge, cardiologist at the health center "Les promoteurs de la bonne santé" for his fruitful advices.

Funding No funding was received.

Compliance with ethical standards

Conflict of interests Pascalin TIAM KAPEN declares that he has no conflict of interest. KOUAM KOUAM Serge Urbain declares that he has no conflict of interest. TCHUEN Ghislain declares that he has no conflict of interest.

Ethical approval This article does not contain any studies with human participants or animals performed by any of the authors.

References

1. Gutierrez A, Lara M, Hernandez PR (2005) A QRS detector based on Haar wavelet, evaluation with MIT-BIH arrhythmia and European ST-T Databases. Computacion y Sistemas. 8:293–302
2. Kaneko M, Gotho T, Iseri F, Takeshita K, Ohki H, Sueda N (2011) QRS complex analysis using wavelet transform and two layered self-organizing map. In: Computing in cardiology. IEEE, New York, pp 813–816
3. Addison PS (2005) Wavelet transforms and the ECG: a review. Physiol Meas 26(5):R155–R199
4. Burke MJ, Nasor M (2002) The time relationships of the constituent components of the human electrocardiogram. J Med Eng Technol 26(1):1–6

5. Schuck A, Wisbeck JO (2003) QRS detector pre-processing using the complex wavelet transform, vol 3. In: Proceedings of the 25th annual international conference of the IEEE engineering in medicine and biology society, 2003. IEEE, New York, pp 2590–2593
6. Vassilikos VP, Mantziari L, Dakos G, Kamperidis V, Chouvarda I, Chatzizisis YS et al (2014) QRS analysis using wavelet transformation for the prediction of response to cardiac resynchronization therapy: a prospective pilot study. J Electrocardiol 47(1):59–65
7. Ieong CI, Mak PI, Lam CP, Dong C, Vai MI, Mak PU et al (2012) 0.83-QRS detection processor using quadratic spline wavelet transform for wireless ECG acquisition in 0.35-CMOS. IEEE Trans Biomed Circuits Syst 6(6):586–595
8. Zeng C, Lin H, Jiang Q, Xu M (2013) QRS complex detection using combination of mexican-hat wavelet and complex morlet wavelet. JCP 8(11):2951–2958
9. Kadambe S, Murray R, Boudreaux-Bartels GF (1999) Wavelet transform-based QRS complex detector. IEEE Trans Biomed Eng 46(7):838–848
10. Hamilton PS, Tompkins WJ (1986) Quantitative investigation of QRS detection rules using the MIT/BIH arrhythmia database. IEEE Trans Biomed Eng 12:1157–1165
11. Okada M (1979) A digital filter for the ors complex detection. IEEE Trans Biomed Eng 12:700–703
12. Jaswal G, Parmar R, Kaul A (2012) QRS detection using wavelet transform. Int J Eng Adv Technol 1(6):1–5
13. Dinh HAN, Kumar DK, Pah ND, Burton P (2001) Wavelets for QRS detection. Aust Phys Eng Sci Med 24(4):207
14. Alvarado C, Arregui J, Ramos J, Pallàs-Areny R (2005) Automatic detection of ECG ventricular activity waves using continuous spline wavelet transform. In: 2005 2nd international conference on electrical and electronics engineering. IEEE, New York, pp. 189–192
15. Manikandan MS, Soman KP (2012) A novel method for detecting R-peaks in electrocardiogram (ECG) signal. Biomed Signal Process Control 7(2):118–128
16. Gutiérrez-Gnecchi JA, Morfin-Magana R, Lorias-Espinoza D, del Carmen Tellez-Anguiano A, Reyes-Archundia E, Méndez-Patiño A, Castañeda-Miranda R (2017) DSP-based arrhythmia classification using wavelet transform and probabilistic neural network. Biomed Signal Process Control 32:44–56
17. Holden AV, Poole MJ, Tucker JV (1995) Reconstructing the heart. Chaos Solitons Fractals 5(3–4):691–704
18. Boyett M, Holden AV, Kodama I, Suzuki R, Zhang H (1995) Atrial modulation of sinoatrial pacemaker rate. Chaos Solitons Fractals 5(3–4):425–438
19. Holden AV, Biktashev VN (2002) Computational biology of propagation in excitable media models of cardiac tissue. Chaos Solitons Fractals 13(8):1643–1658
20. Poole MJ, Holden AV, Tucker JV (2002) Hierarchical reconstructions of cardiac tissue. Chaos Solitons Fractals 13(8):1581–1612
21. Gois SR, Savi MA (2009) An analysis of heart rhythm dynamics using a three-coupled oscillator model. Chaos Solitons Fractals 41(5):2553–2565
22. Tlili M, Maalej A, Romdhane MB, Rivet F, Dallet D, Rebai C (2016) Mathematical modeling of clean and noisy ECG signals in a level-crossing sampling context. In: International symposium on signal, image, video and communications (ISIVC). IEEE, New York, pp 359–363
23. Wu HT, Wu HK, Wang CL, Yang YL, Wu WH et al (2016) Modeling the pulse signal by wave-shape function and analyzing by synchrosqueezing transform. PLoS ONE 11(6):e0157135. https://doi.org/10.1371/journal.pone.0157135
24. Tripathy RK, Mendez AZ, de la Serna JAO, Arrieta Paternina MR, Arrieta JG (2018) Naik GR (2018) Detection of life threatening ventricular arrhythmia using digital taylor fourier transform. Front Physiol 9:722
25. Raj S, Ray KC (2018) Sparse representation of ECG signals for automated recognition of cardiac arrhythmias. Expert Syst Appl 105:49–64
26. Raka AG, Naik GR, Chai R (2017) Computational algorithms underlying the time-based detection of sudden cardiac arrest via electrocardiographic markers. Appl Sci 7(9):954
27. de Albuquerque VHC, Nunes TM, Pereira DR, Luz EJDS, Menotti D, Papa JP, Tavares JMR (2018) Robust automated cardiac arrhythmia detection in ECG beat signals. Neural Comput Appl 29(3):679–693
28. http://samples.jbpub.com/9781449652609/99069_ch05_6101.pdf. Accessed 05 Dec 2018
29. McSharry PE, Clifford GD, Tarassenko L, Smith LA (2003) A dynamical model for generating synthetic electrocardiogram signals. IEEE Trans Biomed Eng 50(3):289–294
30. https://www.physionet.org. Accessed 08 Nov 2018